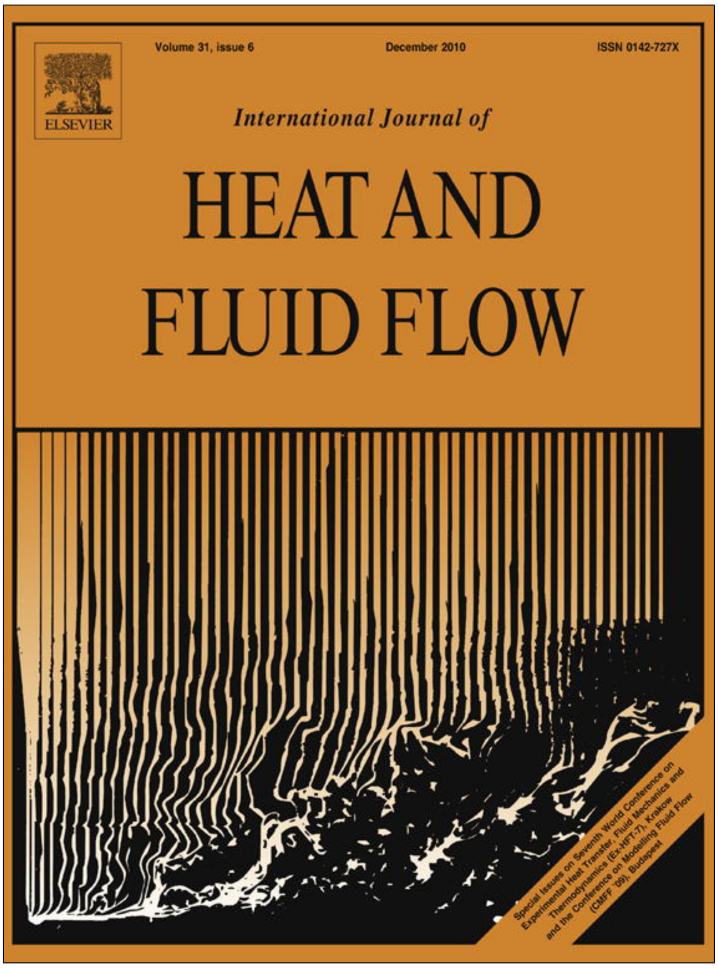
Volume 31, issue 6
December 2010
ISSN 0142-727X
ELSEVIER
International Journal of
HEAT AND
FLUID FLOW
Special Issues on Seventh World Conference on Experimental Heat Transfer, Fluid Mechanics and Thermodynamics (ExHFT-7), Krakow and the Conference on Modeling Fluid Flow (CMFF '09), Budapest

International Journal of Heat and Fluid Flow 31 (2010) 996–1004

Contents lists available at ScienceDirect

International Journal of Heat and Fluid Flow

journal homepage: www.elsevier.com/locate/ijhff

Dynamics of nanofibres conveyed by low Reynolds number flow in a microchannel ☆

K. Sadlej, E. Wajnryb, M.L. Ekiel-Jeżewska, D. Lamparska, T.A. Kowalewski *

IPPT PAN, Polish Academy of Sciences, Pawińskiego 5B, 02-106 Warsaw, Poland

ARTICLE INFO

Article history:
Received 11 September 2009
Received in revised form 8 December 2009
Accepted 17 February 2010
Available online 15 March 2010

Keywords:
Nanofibres suspension
Microchannels
Filament dynamics
Stokesian dynamics
Multipole expansion

ABSTRACT

In this paper we aim to create an experimental and numerical model of nano and micro filaments suspended in a confined Poiseuille flow. The experimental data obtained for short nanofibres will help to elucidate fundamental questions concerning mobility and deformation of biological macromolecules due to hydrodynamic stresses from the surrounding fluid motion. Nanofibres used in the experiments are obtained by electrospinning polymer solutions. Their typical dimensions are 100–1000 μm (length) and 0.1–1 μm (diameter). The nanofibre dynamics is followed experimentally under a fluorescence microscope. A precise multipole expansion method of solving the Stokes equations, and its numerical implementation are used to construct a bead-spring model of a filament moving in a Poiseuille flow between two infinite parallel walls. Simulations show typical behaviour of elongated macromolecules. Depending on the parameters, folding and unfolding sequences of a flexible filament are observed, or a rotational and translation motion of a shape-preserving filament. An important result of our experiments is that nanofibres do not significantly change their shape while interacting with a micro-flow. It appeared that their rotational motion is better reproduced by the shape-preserving Stokesian bead model with all pairs of beads connected by springs, omitting explicit bending forces.

1. Introduction

Microfluidics is a rapidly growing field of basic and applied research, predominantly driven by the tight demands of biotechnology. The well-known lab-on-a-chip (LOC) concept embraces the goal of integrating a bio-laboratory on a single microfluidic chip (Mijatovic et al., 2005). Recent developments of the LOC technology provide possibility for handling not only single cells but to use a microfluidic systems for manipulating, sorting and analysing individual biomolecules. Devices consisting of nanoscale pores are being pursued as probes of molecular structure, as demonstrated by Maleki-Jirsaraei et al. (2007) and Schroeder et al. (2004). Single, double or triple DNA strands passing nanopores were observed by Joo et al. (2008) and Craighead (2006) to extract the identity of DNA bases. In such devices, molecular migration in flowing dilute polymeric solutions is a well-known phenomenon. The chain deformation and migration away from the confined walls greatly affect its transport dynamics, as pointed out by Jendrejack et al. (2004).

Rapid measurements of DNA fragment size, of their folding and unfolding sequences represent challenging target for present single molecule studies. Development and availability of highly sensitive experimental tools permits to follow the transient behaviour of single macromolecules in a nearly native environment. However, such studies are still very tedious and expensive. The available experimental data are mostly quantitative, not accurate enough to be used for validating numerical models. In addition, modelling of microbiological processes involves complex molecular interactions difficult for direct modelling due to prohibitive number of molecules involved and time scales far beyond those available for simulation methods at molecular level (compare Kreuzer and Grunze, 2001 or Dai et al., 2008).

Hence, despite great progress in recent modelling of single DNA molecules in flow (e.g. Mura and McCammon, 2008), there is common agreement that understanding slender filament dynamics in Stokes flow may elucidate fundamental questions about mobility and deformation of biological macromolecules due to hydrodynamic stresses from the surrounding fluid motion. Moreover, by combining hydrodynamic interactions with molecular models one may aim to achieve a multiscale description of biologically driven processes, enormously improving computational efficiency.

From a theoretical point of view, the interest in dilute polymer solutions comes primarily from their importance in understanding the molecular response to hydrodynamic forces free from introducing the complication of molecular interactions. Understanding those classical problems of polymer fluid dynamics has proven useful for many applications. Hence, long-chained polymers have been studied numerically taking into account stretching, bending, twisting and hydrodynamic forces between their segments.

☆ Paper presented on 7th World Conference on Experimental Heat Transfer, Fluid Mechanics and Thermodynamics 28 June–03 July 2009, Krakow, Poland.

* Corresponding author. Tel.: +48 22 8269803; fax: +48 22 8269815.
E-mail address: tkowale@ippt.gov.pl (T.A. Kowalewski).

0142-727X/$ - see front matter
doi:10.1016/j.ijheatfluidflow.2010.02.021

Nomenclature

a	channel depth (mm)
A	bending stiffness (–)
d	fibre diameter, beads diameter (μm)
h	distance between walls, fibre diameter units (–)
H	distance between walls (mm)
k	extensional elasticity (–)
l_0	initial beads distance in fibre diameter units (–)
N	number of beads, relative length of the fibre
Re	Reynolds number based on beads diameter = $\rho U d/\eta$
$\boldsymbol{u}$	flow field in the channel (–)
U	mean flow velocity (m/s)
v	maximum flow velocity (where $U = v/2$)
x	coordinate along the channel, distance in fibre diameter units
y	coordinate along the channel depth
z	coordinate across the channel, distance from the wall in fibre diameter units
η	dynamic viscosity of the fluid (Pa s)
ρ	density of the fluid (kg/m^3)

Normalisation is based on the length d and the maximal velocity v, time is scaled by d/v and force is scaled by $\pi\eta v d$

Several simulation techniques have been applied to investigate motion of flexible filaments in a fluid flow. Szymczak and Cieplak (2007) investigated unfolding of proteins using the coarse-grained molecular model combined with hydrodynamic interactions. Usta et al. (2007) studied transversal motion of polymers using lattice-Boltzmann method. The finite-difference numerical model was used by Lindström and Uesaka (2007) to simulate the motion of flexible fibres in viscous flow.

Different models of segment shape and the hydrodynamic interactions between them have been applied. Finitely extensible nonlinear elastic dumbbell (FENE) model is commonly used in modelling polymer solutions (see Purnode and Crochet, 1998). Park and Butler (2009) pointed out importance of Brownian motion for describing dynamics of nano and micro-scale filaments in flow. Yamamoto and Matsuoka (1993) proposed a method of modelling fibre made of bonded spheres to study its dynamics in creeping flow regime. Shelly and Ueda (2000) and Tornberg and Shelley (2004) took into account hydrodynamic interactions between the fibre segments within the slender body theory, and Gauger and Stark (2006) within the Rotne–Prager approximation. The accurate multipole calculation of hydrodynamic interactions between the beads modelling rod-like particles entrained by the Poiseuille flow in parallel-wall geometry was carried out by Zurita-Gotor et al. (2007), Bhattacharya et al. (2005), and Blawzdziewicz et al. (2005).

In recent years, with the increase of experimental data, computer speed and development of numerical and theoretical methods, polymer simulations achieved with ensembles of coarse-grained chains have become promising. On the other hand, the coarse, long time scale behaviour of elongated macromolecules can be usually relatively well described using a suitable theoretical model of interactions between the polymer segments, implemented numerically using an efficient computational method. Having all the above arguments in mind the present paper aims to create an experimental and numerical model allowing to obtain quantitative data on hydrodynamics of nano and microfilaments suspended in a confined Poiseuille flow. Experimental microscopic observation data are obtained for the fluid – filament interactions. To evaluate the importance of hydrodynamic interactions a hydrodynamic model describing dynamic behaviour of a single fibre in a Poiseuille flow is proposed. It includes lateral migration, rotation, wall effects, and possibly also folding–unfolding sequences of fibres conveyed by the flow.

2. Experimental

The main part of the experimental set-up consists of a microscope, a light source, a high-speed digital camera, and a microchannel. The flow of single fibres suspended in water is recorded using the epi-fluorescence microscope (Nikon Eclipse 50i) equipped with 10× (NA 0.3/WD 17.30 mm) lens covering an area of 854 μm × 683 μm. The high pressure mercury lamp (Nikon, LHM 100C1) is mainly used for illuminating slow motion. Short illumination time is achieved by using a single pulsed Nd:YAG laser, delivering 1 m J energy at 532 nm wavelength and 1 kHz repetition rate (Ekspla Ltd.). The flow is illuminated and observed through the upper wall of the microchannel. The microscope lens is focused in the mid-plane of the channel. The depth of focus limits observations to about 10 μm thick layer. Hence, fibres traversing too close to the bottom or top walls are out of focus and not considered for further evaluation. By traversing the field of observation in the horizontal and vertical direction, the position of the interrogated flow plane is selected. A high-speed 10 bit PCO 1200HS camera with 1280 × 1024 pixels resolution is used for recording flow images. The suspending medium is distilled and deionized water. Experiments are performed at room temperature. In most cases, the flow is driven by the syringe micro-pump (NE1000, IITC Life Science Inc.) permitting flow rate variation from 0.03 mm^3/s to 40 mm^3/s. The typical flow velocity in this study is below 100 μm/s. Hence, the Reynolds number of the flow based on the fibre diameter is in all investigated cases much smaller than unity ($Re < 10^{-4}$).

The micro and nano filaments used in the experiment are produced by electrospinning polymer solutions, as described by Kowalewski et al. (2005). Two types of polymers, polycaprolactone (PCL) and poly-L-lactide (PLLA), are used to form short, insoluble in water filaments. Density of the polymers is close to that of water (1130 kg/m^3 and 1270 kg/m^3). The settling velocity in water for a typical fibre used in the study is <1 μm/s. Hence, the buoyancy effects are assumed to be negligible.

Small amount of rhodamine is added to the polymer solution to make produced filaments visible under the fluorescence microscope. Once fibres are exposed to 532 nm green light from the laser, they emit red light with an emission maximum at 612 nm. The low pass filters, mounted between the objective and the camera permit only the fluorescent red light to pass, while preventing the illuminating green light to be detected by the camera. It permits to isolate images of fibres from the background light and helps to visualize objects with size below resolution limits of the optical microscopy. For visualization of the channel slight background illumination is in some cases additionally applied.

The flow is studied in channels created in a PDMS mould, and in a straight channel formed between two glass plates separated by a thin Teflon film. The typical channel width is 1 mm. By modifying electrospinning parameters it is possible to produce filaments of diameters varying from 100 nm to 5 μm. The aspect ratio of filaments varies from 50 to several thousands. In fact it is difficult to obtain short pieces of filaments and several scenarios of microfluidic separators are applied to preselect randomly chopped continuous nanofibres before they are used in the experiment. For this

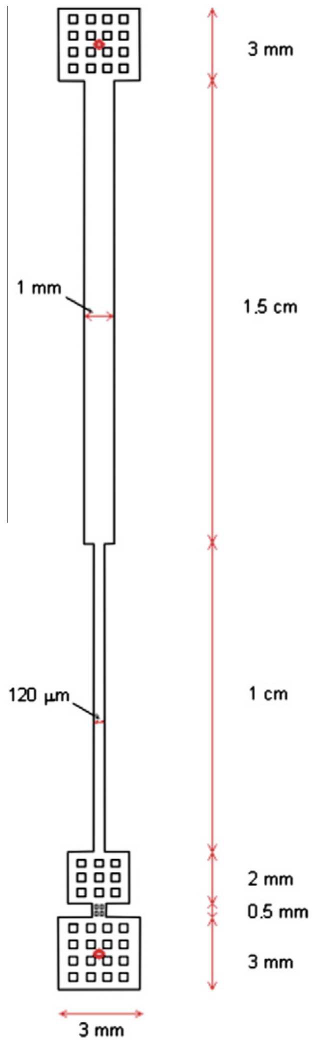

Fig. 1. Schematic of the microchannel with pillars used for studying nanofibre translocation in the flow.

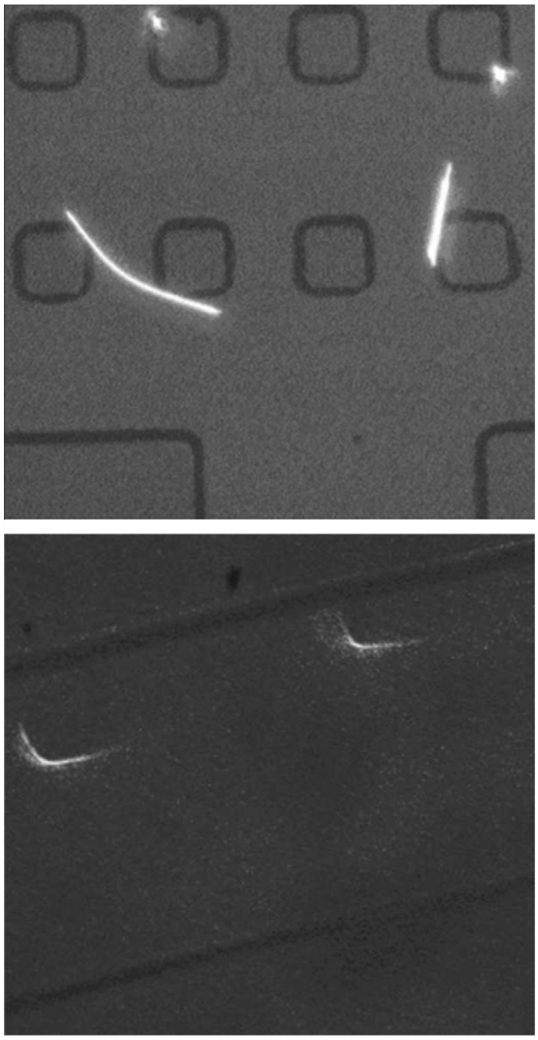

Fig. 2. Fluorescent filaments passing multi-pillar separator (top), and conveyed close to the channel wall (bottom). Image width corresponds to 0.3 mm.

purpose the multi-pillar separators present at the channel entrance (Fig. 1) help us to trap long fibres before they enter straight part of the channel.

Fluorescent light from filaments suspended in the flow is collected by the camera at given time steps. Translocation of filaments within the channel and their shape evolution are evaluated using image processing software. To obtain quantitative data on the fibre shape we extract and analyse the fibre profile for each frame of the recorded movie. Than, the fibre contours are digitized pixel by pixel using tracking software and the collected points are fitted to the 7th order polynomial. This polynomial is used to generate the predefined initial configuration for the numerical simulations.

Fig. 1 shows typical shape of the PDMS microchannel used for investigating single fibre dynamics. The straight parts of the microchannel allow for studying fibre interaction with a Poiseuille flow, structured obstacles in form of pillars are used to analyse possibility of fibre sorting. Preliminary experiments with single nanofibres are performed to collect knowledge about different flow scenarios. Steady and pulsating flow is generated to analyse behaviour of suspended nanofibres. In most cases after single nanofibre is localized in viewing area of the camera, the flow is stopped and reversed. Such push–pull motion permits us to observe selected object without changing position of the channel.

Figs. 2 and 3 show examples of collected images of nanofibres acquired under the fluorescent microscope. The motion of short (0.2 mm) fragments through the multi-pillar structure (Fig. 2 (top)) exhibits characteristic fibre bending. For longer fragments (above 0.5 mm) looping of the fibre tails is observed. This behaviour shows several similarities to confinement-induced coiling–recoiling of DNA molecules studied by Doyle et al. (2000). When flowing through the pillars fibres exhibit snake like deformations meandering between obstacles and finally they are trapped between them. They could not be removed by pressure driven flow. This effect can be used to sort out selected fibre fragments before they enter the straight part of the microchannel. This technique of fibres separation mimics experiments performed by Bruin (2000) for large DNA molecules passing through array of micropillars. Our micro-scale experimental data describing behaviour of filaments passing the multi-pillar structure can be used to analyse the performance of numerical models constructed to described such flows (comp. Maleki-Jirsaraei et al., 2007).

Simple geometry, like straight channels are used to validate hydrodynamic models. It is found that in our experiments fibres conveyed through the straight channel usually are already deformed by the initial flow shear stresses (comp. Figs. 2 and 3). These deformations appear to remain almost unchanged for the level of shear stresses generated by the flow in our straight channels, thus

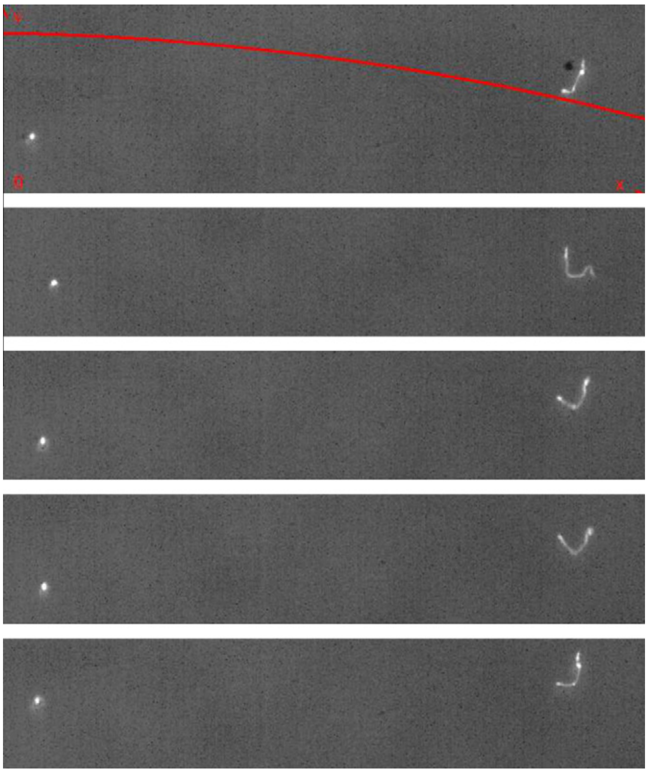

Fig. 3. A sequence of images of a nanofibre conveyed by a Poiseuille flow. The microchannel width is 2 mm and the mean flow velocity is 40 μm/s. Channel axis is on the left side; less than one half of the channel is visible. Poiseuille velocity profile is indicated in the top slide. The bright spot on the left is a fluorescent particle used to measure local flow velocity.

rather tumbling, rotating type of fibre motion is observed. An example of such behaviour gives Fig. 3. The sequence of images is extracted from the longer movie and illustrates dynamics of nanofibre fragment located about 40 μm from the channel wall. It is interesting to note, that the average velocity of the fibre is similar to that of a tracer particle located close to the flow axis (Fig. 3). By tracing displacement of both tails of the tangled fibre it is found that in this case, the part being closer to the wall is apparently nearly 20% faster than the other one. This leads to counter-clockwise rotation of the structure, in opposition to single particle rotation exhibited for the shear flow. This unintuitive behaviour is probably caused by the closed geometry of the channel, and the non-negligible effect of the three-dimensional variation of the flow.

In the next chapter, two examples of configurations observed for the straight channel flow, namely a fibre close to the wall and a fibre close to the flow axis, are extracted from the experimental movies and compared with our numerical models. In this case, the two-dimensional flow seems to be a good approximation for the observed behaviour of the fibre.

3. Numerical

The bead-spring model is used here to simulate the dynamic behaviour of fibres. A fibre consists of a sequence of beads, connected by springs, which do not contribute to the frictional interaction but are responsible for the elastic and deformational properties of the chain. The beads offer a hydrodynamic resistance to the flow of the surrounding medium. The chain of beads is conveyed by Poiseuille flow inside a microchannel modelled by two infinite parallel-walls (Fig. 4).

The regime of low Reynolds number (based on the particle size) is considered and the Brownian motion of particles is neglected,

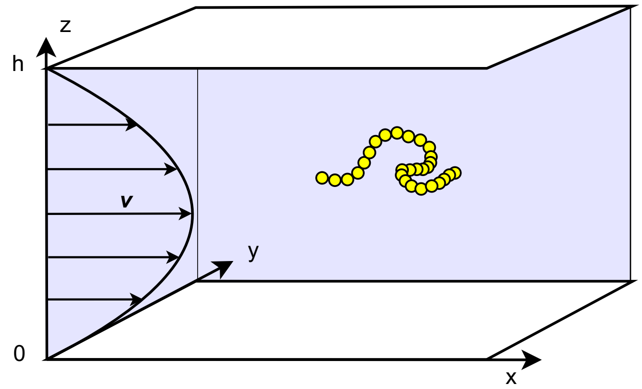

Fig. 4. Coordinate system of the numerical model.

resulting in a flow description based on the stationary Stokes equations

$$\begin{aligned} &\eta \nabla^2 \boldsymbol{u} - \nabla p = 0, \\ &\nabla \cdot \boldsymbol{u} = 0, \end{aligned} \tag{1}$$

where η is the fluid viscosity, p is the pressure and $\boldsymbol{u}$ is the fluid velocity field. These equations are supplemented by no-slip boundary conditions for the fluid velocity field on the filament and the wall surfaces, as well as the condition of vanishing disturbance of the Poiseuille fluid flow far away from the fibre. In the model adopted, each fibre strand is constructed out of N solid non-deformable spherical particles which can move with respect to each other. Two models of interactions between the beads are considered, a flexible filament (FF) model and a shape-preserving, elastic filament (EF) model.

In the flexible filament model (FF), the spheres are lined up and the closest neighbours are connected by fictitious Fraenkel springs obeying Hook's law with equilibrium length l_0, a parameter of the model describing initial distance between beads. Although the total external, non-hydrodynamic force and torque applied to the fibre are absent, each bead of the fibre feels stretching and bending forces discretised as described by Gauger and Stark (2006)

$$\begin{aligned} \boldsymbol{F}_i^s &= k(r_{i-1,i} - l_0)\hat{\boldsymbol{r}}_{i-1,i} - k(r_{i,i+1} - l_0)\hat{\boldsymbol{r}}_{i,i+1}, \\ \boldsymbol{F}_i^b &= -\frac{A}{2l_0}\nabla_{\boldsymbol{r}_i}\sum_{k=1}^{N}\left(\hat{\boldsymbol{r}}_{k+1,k} - \hat{\boldsymbol{r}}_{k,k-1}\right)^2, \end{aligned} \tag{2}$$

where k is the stretching force constant (second parameter of the model), $\boldsymbol{r}_i$ is the position of the centre of bead i, $\boldsymbol{r}_{ij}$ is a vector of length r_{ij} connecting the centre of sphere j with the centre of sphere i, with the corresponding unit vector $\hat{\boldsymbol{r}}_{ij} = \boldsymbol{r}_{ij}/r_{ij}$ and the initial distance between the neighbouring spheres is l_0. Here, A denotes the bending stiffness (flexibility) constant. All quantities are non-dimensional. Distances are measured in particle diameter d, and forces in the units $f_0 = \pi\eta d v$, where v is the maximal velocity of the ambient Poiseuille flow. Therefore, the stretching force constant k and the bending stiffness A are dimensionless parameters, which estimate the strength of the stretching and bending forces relative to the hydrodynamic force exerted by the fluid flow.

In the shape-preserving elastic fibre (EF) model, the filament remembers its initial shape, although it is not stiff and can stretch and bend. Explicit bending forces are absent in this model, and the stretching forces are now applied to all pairs of the beads, not only the nearest neighbours,

$$\boldsymbol{F}_i^s = -k\sum_{j \neq i}^{N}(r_{ij} - r_{0ij})\hat{\boldsymbol{r}}_{ij}. \tag{3}$$

In the Stokes flow regime, there is no inertia and the external forces are balanced by forces resulting from hydrodynamic inter-

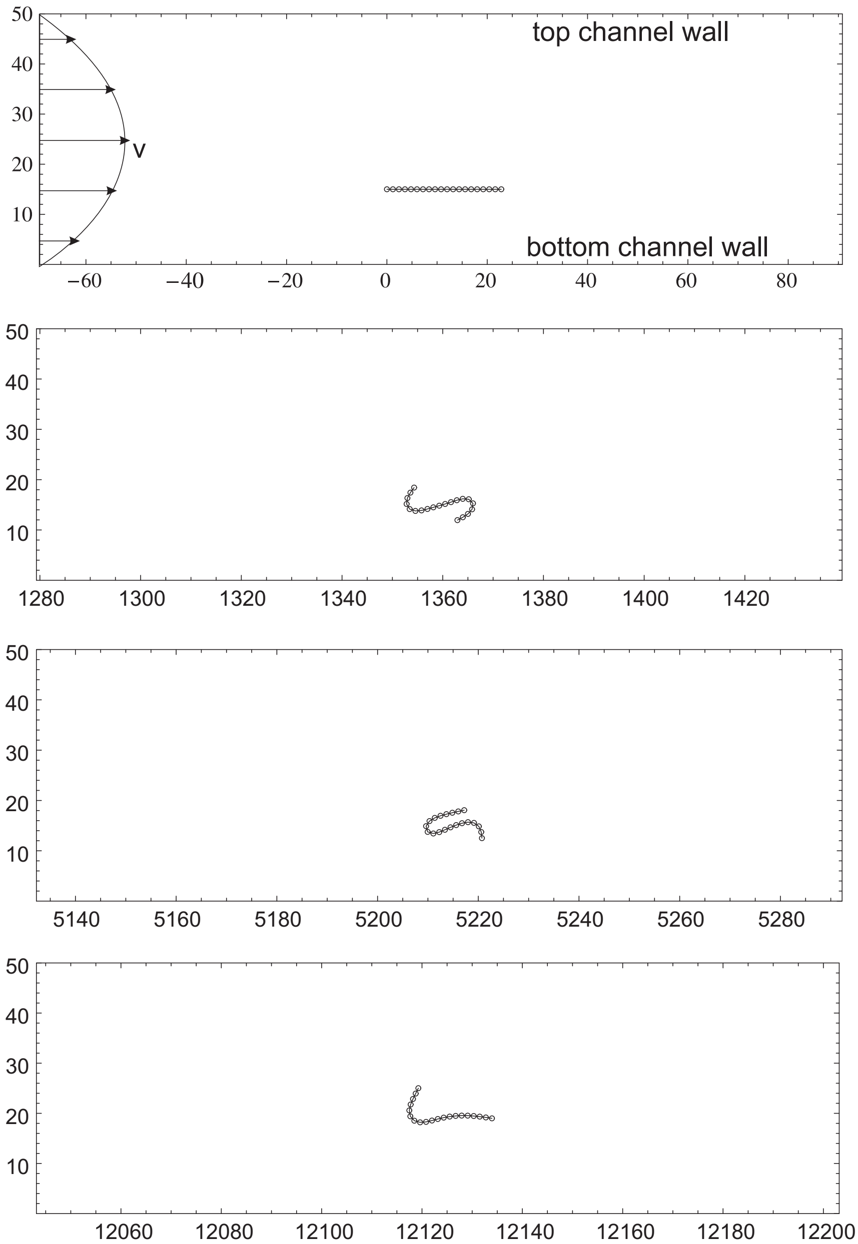

Fig. 5. Numerical modelling: flipping/tumbling motion of a fibre conveyed along the channel wall. Travelled distance is given in fibre diameter units; initially the fibre is straight and aligned with the flow at a distance from the wall $z = 15$. Number of beads $N = 20$, distance between the walls $h = 50$ (fibre diameter units). The model parameters are: $l_0 = 1.2,\ k = 10,\ A = 0.5$..

actions between segments of the fibre through the flow itself. The following procedure is used to derive dynamical behaviour of the fibre. For each fixed configuration the instantaneous hydrodynamic forces exerted by the fluid on the motionless particles (beads) are calculated. The velocity of each bead is linearly proportional, through the mobility matrix dependent on the exact position of all fibre segments, to the sum of these forces and to the elastic and bending forces exerted on each fibre segment. Both the hydrodynamic forces and the mobility matrix are determined numerically by the HYDROMULTIPOLE algorithm, described by Ekiel-Jeżewska and Wajnryb (2006). It implements the theoretical multipole method of Cichocki et al. (2000) for calculating hydrodynamic interactions between bodies within a Stokesian dynamics. In this scheme, hydrodynamic interactions between the close surfaces of the beads are accurately evaluated owing to the lubrication correction. The cut-off parameter $L = 2$ for the multipole method is used. It means that $3L(L + 2) = 24$ multipole moments are calculated for each of the N beads used to model the fibre. It is sufficient to obtain correct results. For a discussion of precision, refer to Ekiel-Jeżewska and Wajnryb (2006).

The wall–fibre interactions are incorporated by the single wall superposition of hydrodynamic forces for the two-wall system (see Zurita-Gotor et al., 2007, Bhattacharya et al., 2005), in contrast to the superposition of Green functions corresponding to the lower and upper wall. Our approximation would not be very accurate for narrow channels when the longitudinal dimension of the fibre is larger then the width of the channel, but it performs very well for channels as wide as those used in the experiments. Here we consider the case of relatively wide channels compared to the fibre length, hence the use of single wall superposition approximation is fully justified and gives precise results. The evolution of the fibre is

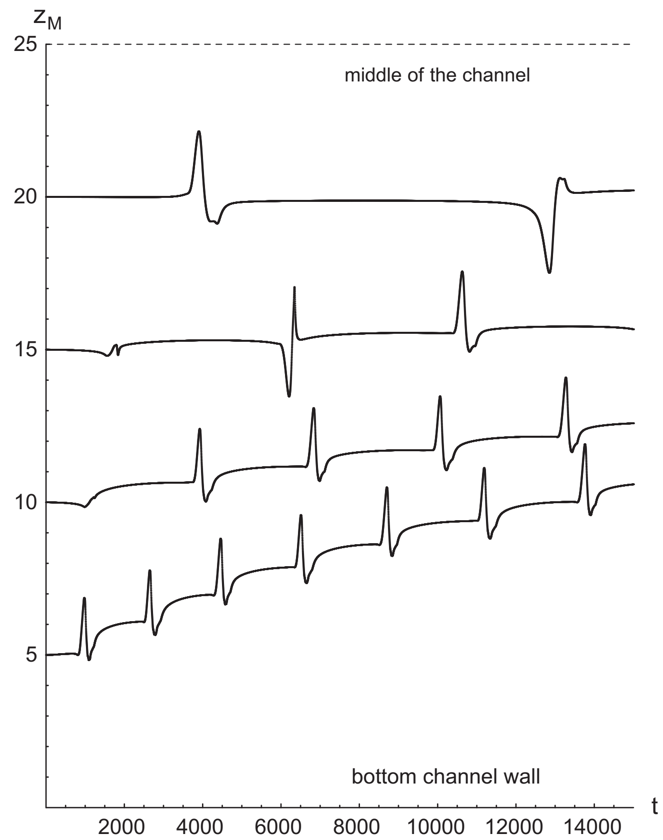

Fig. 6. Migration of fibres from different initial positions towards the middle of the channel. Depicted is the time dependent position z_M of the middle of a $N = 20$ beads long fibre. At $t = 0$ the fibres are straight and aligned with the flow. The peaks at each of the curves correspond to a flip of the fibre. The channel height is $h = 50$. Other parameters take values $l_0 = 1.2,\ k = 10,\ A = 0.5$.

determined by time stepping the set of coupled differential equations for each fibre segment position.

Parametric simulations have been performed to test performance of the FF and EF models. Hence, we have investigated behaviour of the flexible filament in the Poiseuille flow, tracing such processes like deformation of the filament shape, periodic orbits, and cross-flow migration, keeping in mind that for very high shear rates nanofibres are expected to fold, changing their shape significantly. The general investigation of flexible filaments has been carried out within the FF model for several initial configurations, different fibre aspect ratios (number of beads) and different values of the bending stiffness A. A typical fibre evolution with snake like turns and coiling is shown in Fig. 5. Very similar behaviour was observed by Forgacs and Mason (1959a,b) in their experiments with flowing elastomer fibres.

Several simulation runs performed for short strings of beads conveyed by Poiseuille flow gave us interesting conclusions summarized below (the details will be presented elsewhere):

1. The motion of a single fibre strand in the Poiseuille flow simulated with FF model shows a generic behaviour. Independently of the initial configuration, it fairly rapidly (depending on its length and degree of entanglement), straightens out along the streamlines. It than begins a flipping or tumbling motion, which is almost periodic. Almost, not exactly, because the fibre has a tendency to migrate away from the wall, moving through areas of different flow velocities as shown in Fig 6. This behaviour has been seen in previous simulations by Usta et al. (2007). The elastic fibre (EF) model is characterized by high bending stiffness. Hence, it allows for rotation but preserves initial fibre shape.
2. Migration of fibres towards the centre of the channel is present only when the initial distance from the wall is large enough (typically larger then approximately 5 fibre diameters). When fibres are closer to the wall, its presence hinders their flipping, and what follows, also their migration. The migration speed decreases with distance from the wall (comp. Fig 6). The main mechanism of migration is the variation of shear rate coupled with the flexibility of the fibres.
3. Greater stiffness of the fibre hinders flipping on small distances from the wall and increases the flipping period elsewhere. On the other hand the flipping period of a straight fibre obtained with EF model with incorporated shape stiffness appears to be almost the same as that of FF model for equivalent configuration.
4. Longer fibres migrate faster towards the middle of the channel and take much longer time to flip while bending. A short fibre behaves as a solid rod rotating in the flow for both models. A long flexible fibre (FF model) exhibits nearly periodic stretching and winding (comp. Fig. 5).

In the following chapter we give examples of comparison of both models with selected configurations extracted from the present experiments.

4. Comparison of the FF and EF models with the experiment

The second part of our numerical analysis is focused on modelling the motion of nanofibres detected by our camera. Using measured data for the initial shape of a fibre we performed simulations for the flow conditions similar to the experimental ones. Both models FF and EF are tested and results obtained for optimized parameters are compared with the corresponding images of the flowing fibre. As mentioned before, the two examples of configurations observed for the straight channel flow, namely fibre close to the wall and fibre close to the flow axis are considered.

The first analysed sequence is shown in Fig. 7 (top). It illustrates the evolution of a short nanofibre moving close to the wall at the non-dimensional distance $z/h = 0.17$. The flow is from left to right with the average velocity $U = 40\ \mu\text{m/s}$. The fibre diameter is $d = 1\ \mu\text{m}$, and the rectangular cross-section of the channel has the following dimensions: width $H = 2$ mm, and depth $a = 1.2$ mm. The initial C-shape of the fibre is preserved during our short observation time (3.4 s). The fibre rotates counter-clockwise changing during this time its orientation by nearly 90°.

To reproduce this behaviour, the flexible fibre (FF) numerical model was used, starting from the initial configuration observed in the experiment, with $N = 37$ beads, located at equal distances along the fibre shape, which was obtained by a polynomial interpolation of the experimental data points. The model parameters were chosen to represent a very close ($l_0 = 1.001$) bead-packing and a high fibre stiffness ($k = 10, A = 10$). As shown in Fig. 7 (middle raw), the initially C-shaped fibre ($t = 0$) after a short time ($t = 1$ s) becomes nearly straight and in general inclined with respect to the flow direction. The results of the simulation show that after approximately 10 s the fibre straightens out and later moves parallel to the wall for a long time. It remains straight for over 100 s flow time, when suddenly it turns ($t = 105$ s), changing its orientation to almost perpendicular to the wall. The fibre becomes slightly deformed at the upward position ($t = 111$ s), and than quickly flips the next 90° to become again a straight fibre elongated with the flow.

As such behaviour obviously is different from the experiment, the second model with increased stiffness (EF) is applied. Assuming the same model parameters (values of k and l_0), the second simulation starts from the same initial position ($t = 0$) of the C-shaped fibre

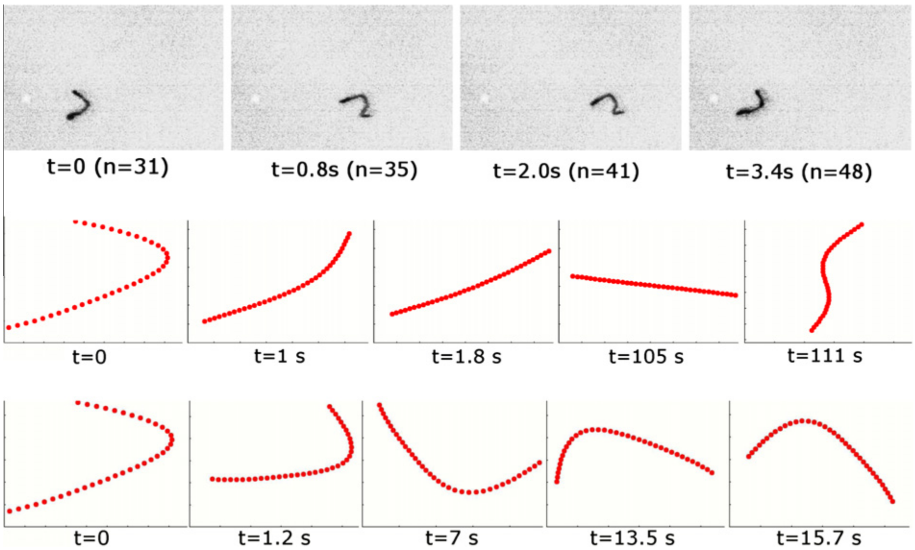

Fig. 7. Evolution of a short nanofibre moving close to the wall $(z/h = 0.17)$ – comparison of the experiment with two numerical models. The flow is from left to right. $U = 40$ μm/s, $d = 1$ μm, $H = 2$ mm. Simulation parameters: $k = 10,\ l_0 = 1.001,\ A = 10,\ N = 37$. (Top) Images extracted from the experiment. The frame number (n) and time (t) are indicated below the images. The *C*-like fibre keeps its shape almost unchanged, rolling during the observation time by 90° only. The fibre rotates counter-clockwise. The apparent shape changes are interpreted as the optical projection. (Middle) Numerical folding fibre (FF) model. The height of the plots corresponds to about a 30 μm section of the channel. The fibre rotates clockwise, the flow is from left to right. The initial *C*-like shape changes with time. The fibre aligns with the flow, then after a long time it quickly flips and remains elongated again. During flipping, when the fibre is oriented across the flow, it becomes deformed, but its shape does not coincide with the initial condition. Flipping period is approximately 115 s. (Bottom) Numerical elastic fibre (EF) model. The height of the plots corresponds to about a 30 μm section of the channel. The fibre rotates clockwise, the flow is from left to right. The initial *C*-shape remains preserved with only minor modifications. The fibre flips with a period of approximately 17.5 s.

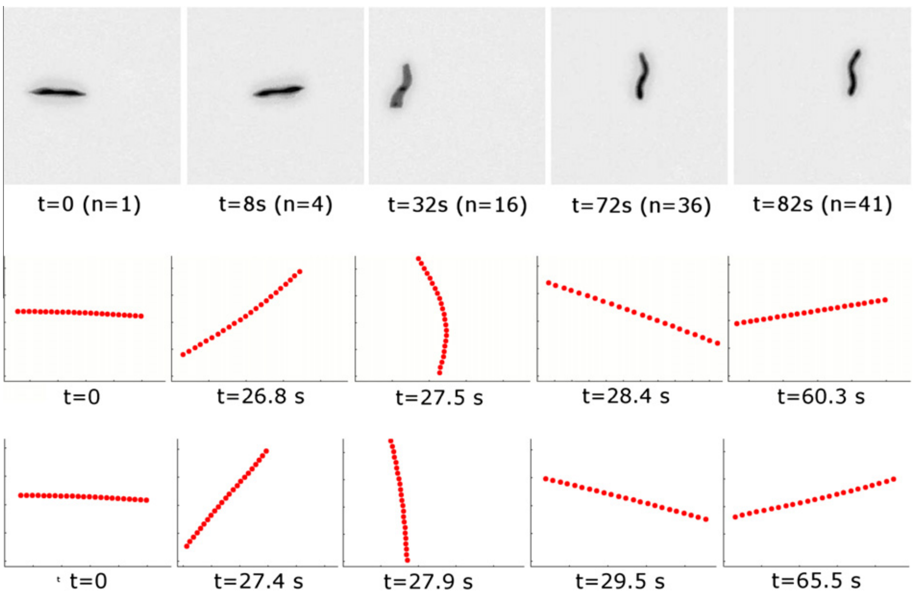

Fig. 8. Evolution of a short nanofibre close to the flow axis – comparison of the experiment with two numerical models $(z/h = 0.63)$. The flow is from left to right. $U = 12.6$ μm/s, $d = 1.5$ μm, $H = 850$ μm. Time is indicated below the images. The simulation parameters are: $k = 10,\ l_0 = 1.001,\ A = 10,\ N = 23$. (Top) Images extracted from the experiment, the frame number (n) and the time instant (t). The fibre is initially elongated with the flow. After a relatively short time it quickly flips to the vertical (cross-flow) position and remains there for a long time, rolling along its axis. Fibre rotates counter-clockwise. The *S*-shape of the fibre was probably present also in the first image but it may be hidden by the optical projection. (Middle) Numerical folding fibre (FF) model. Fibre rotates counter-clockwise. The fibre is initially elongated with the flow and after a long time slightly bends, than quickly flips (27 s). It remains elongated again until the next flipping occurs. The full flipping period is approximately 60 s. (Bottom) Numerical elastic fibre (EF) model. Fibre rotates counter-clockwise. The fibre is initially elongated with the flow, after a long time it quickly flips and remains elongated again. The flipping period is approximately 60 s.

in the flow (comp. Fig. 7 bottom raw). According to the EF model, the *C*-shaped fibre preserves its shape and within a relatively short time $(t = 13$ s) it rotates 90° clockwise. After a longer time it flips and comes back to the initial orientation, only slightly migrating from the wall across the channel. The full flipping period for this case is 17.5 s. This simulation result is qualitatively much closer to the experimental findings. However the experimentally observed period of rotation is nearly five times shorter.

The second analysed experimental case is shown in Fig. 8 (top). The evolution of a short nanofibre of the diameter $d = 1.5$ μm in the rectangular channel having width $H = 0.85$ mm and depth $a = 1.2$ mm is recorded at the 2 s time intervals. The flow is from left to right, with the mean velocity $U = 12.6\ \mu m/s$. The fibre is slightly out of the channel axis ($z/h = 0.63$) and rotates counterclockwise. The initially straight shape of the fibre is preserved during the whole observation time. The slight shape variations visible in the images are probably due to its rotation in the third dimension. The fibre is initially oriented parallel to the flow streamlines, but after about 32 s suddenly flips uprights, i.e. perpendicularly to the walls. This orientation seems to be stable for the next 40 s, and analysing all frames of the movie one gets the impression that the fibre rotates along its axis.

To reproduce the fibre evolution, the flexible fibre (FF) numerical model was started using initial configuration from the experiment. The model parameters are the same as before, i.e. very close packing of the beads ($l_0 = 1.001$) and high fibre stiffness ($k = 10, A = 10$). The fibre length defined by the number of beads is $N = 23$. As shown in Fig. 8 (middle), the initially straight fibre elongated with the flow ($t = 0$) keeps its shape nearly unchanged for the whole time of the simulation, flipping with the period of about 70 s. A slight fibre deformation is visible only at the upward (cross-flow) position ($t = 27.5$ s). It is worth noting that the upward orientation is highly unstable for a straight fibre; the fibre flips 180° from a parallel to the wall orientation to the anti-parallel one during less than 2 s.

Very similar behaviour is obtained for the second simulation (Fig. 8 (bottom)), based on the EF model. The main difference between both simulations is a smaller fibre deformation for the upward position ($t = 27.9$ s) observed in the EF model.

Both simulation results are only qualitatively comparable with the experiment; the flipping sequence differs. Whereas in the experiment the fibre remains parallel to the flow axis for a short time only, staying for the relatively long time in the upward position, the numerical prediction is just the opposite. These and previous discrepancies may have several explanations. The flow in the experimental channel is bounded by four walls and the fibre rotation is influenced by the three-dimensional velocity profile as well as the wall effects of four walls of the channel. Hence, one may expect possible variations of the fibre orientation due to the complex hydrodynamic interactions with the walls. These effects are not included in the model. In addition, only projection of the observed fibre motion is analysed. In the numerical simulation we assume that this projection represents a fibre which is always located within the plane perpendicular to the side walls. In the experiments, three-dimensional orientation of the fibre within the channel is unknown and may be quite different from the in-plane orientation assumed in the simulations.

5. Conclusions

The behaviour of nanofibres conveyed along a microchannel by the Poiseuille flow was analysed under the fluorescence microscope. It appeared that nanofibres of different shapes did not deform significantly while rotating and translating. The essential features of their motion were modelled by the EF spring-bead model. The main results of our investigation can be summarized in the following way:

1. Initially linear filaments practically do not deform while rotating and translating in Poiseuille flow, if the FF model with a sufficiently large bending stiffness A and extensional elasticity k is applied. Most of the time, the fibre remains stretched along flow streamlines. Only from time to time it quickly flips reversing its orientation. During this fast orientation reversal, some shape deformations are observed for this model. Similar behaviour can be found for the EF model with a sufficiently large constant k. However, the experimental flipping period is much shorter if a shape deforms.
2. For a model of a flexible fibre (FF), the initially deformed shape relaxes quite fast to the equilibrium shape of a straight linear filament whatever are the model parameters A and k. Therefore, for non-straight stiff shapes, the FF model cannot explain the results of our experiments. In contrast, the EF model preserves the initial fibre shape once the constant k is sufficiently high. Therefore the EF model accounts much better for the shape-preserving evolution of a C-like fibre observed experimentally.
3. For the flow conditions of the present experiments, i.e. low flow shear stresses, short and relatively stiff fibres which practically do not change their shapes, it appears to us that the EF model better reproduces motion of both bended and straight nanofibres.

We may conclude that our preliminary experimental and numerical studies demonstrate the possibility of measuring and evaluating the dynamics of long microfilaments conveyed by the Poiseuille flow. Further study is planned to elucidate details necessary for quantitative analysis of the fibre dynamics.

Acknowledgements

This investigation was supported by the Polish Ministry of Science and Education program Biowizja. The authors thank Krzysztof Zembrzycki and Sławomir Błoński for their invaluable help in the experimental work.

References

Bhattacharya, S., Blawzdziewicz, J., Wajnryb, E., 2005. Many-particle hydrodynamic interactions in parallel-wall geometry: Cartesian-representation method. Physica A 356, 294–340.
Blawzdziewicz, J., Wajnryb, E., Given, J.A., Hubbard, J.B., 2005. Sharp scalar and tensor bounds on the hydrodynamic friction and mobility of arbitrarily shaped bodies in Stokes flow. Phys. Fluids 17, 033602.
Bruin, G.J.M., 2000. Recent developments in electrokinetically driven analysis on microfabricated devices. Electrophoresis 21, 3931–3951.
Cichocki, B., Jones, R.B., Kutteh, R., Wajnryb, E., 2000. Friction and mobility for colloidal spheres in a Stokes flow near a boundary: the multipole method and applications. J. Chem. Phys. 112, 2548–2561.
Craighead, H., 2006. Future lab-on-a-chip technologies for interrogating individual molecules. Nature 442, 387–393.
Dai, L., Mu, Y., Nordenskio, L., van der Maarel, J.R.C., 2008. Molecular dynamics simulation of multivalent-ion mediated attraction between DNA molecules. Phys. Rev. Lett. 100, 118301.
Doyle, P.S., Ladoux, B., Viovy, J.-L., 2000. Dynamics of a tethered polymer in shear flow. Phys. Rev. Lett. 84, 4769–4772.
Ekiel-Jeżewska, M.L., Wajnryb, E., 2006. Accuracy of the multipole expansion applied to a sphere in a creeping flow parallel to a wall. Q. J. Mech. Appl. Math. 59, 563–585.
Forgacs, L., Mason, S.G., 1959a. Particle motions in sheared suspensions. IX. Spin and deformation of threadlike particles. J. Colloid Sci. 14, 457–472.
Forgacs, L., Mason, S.G., 1959b. Particle motions in sheared suspensions. X. Orbits of flexible threadlike particles. J. Colloid Sci. 14, 473–491.
Gauger, E., Stark, H., 2006. Numerical study of a microscopic artificial swimmer. Phys. Rev. E 74, 021907.
Jendrejack, R.M., Schwartz, D.C., de Pablo, J.J., Graham, M.D., 2004. Shear-induced migration in flowing polymer solutions: simulation of long-chain DNA in microchannels. J. Chem. Phys. 120, 2513–2529.
Joo, C., Balci, H., Ishitsuka, Y., Buranachai, C., Ha, T., 2008. Advances in single-molecule fluorescence methods for molecular biology. Annu. Rev. Biochem. 77, 51–76.
Kowalewski, T.A., Błoński, S., Barral, S., 2005. Experiments and modelling of electrospinning process. Bull. Pol. Acad. Sci.: Technol. Sci. 53, 385–394.
Kreuzer, H.J.M., Grunze, M., 2001. Stretching of single polymer strands: a first-principles theory. Europhys. Lett. 55, 640–646.
Lindström, S.B., Uesaka, T., 2007. Simulation of the motion of flexible fibres in viscous fluid flow. Phys. Fluids 19, 113307.
Maleki-Jirsaraei, M., Sarbolouki, N., Rouhani, S., 2007. Simulation of DNA electrophoresis through microstructures. Electrophoresis 28, 301–308.
Mijatovic, D., Eijkel, J.C.T., van den Berg, A., 2005. Technologies for nanofluidic systems: top–down vs. bottom–up a review. Lab Chip 5, 492–500.
Mura, C., McCammon, J.A., 2008. Molecular dynamics of a κB DNA element: base flipping via cross-strand intercalative stacking in a microsecond-scale simulation. Nucleic Acids Res. 36, 4941–4955.
Park, J., Butler, J.E., 2009. Inhomogeneous distribution of a rigid fibre undergoing rectilinear flow between parallel walls at high Peclet numbers. J. Fluid Mech. 630, 267–298.

Purnode, B., Crochet, M.J., 1998. Polymer solution characterization with the FENE–P model. J. Non-Newton Fluid Mech. 77, 1–20.
Schroeder, C.M., Shaqfeh, E.S.G., Chu, S., 2004. Effect of hydrodynamic interaction on DNA dynamics in extensional flow: simulation and single molecule experiment. Macromolecules 37, 9242–9256.
Shelly, M.J., Ueda, T., 2000. The Stokesian hydrodynamics of flexing, stretching filaments. Physica D 146, 221–245.
Szymczak, P., Cieplak, M., 2007. Influence of hydrodynamic interactions on mechanical unfolding of proteins. J. Phys.: Condens. Matter 19, 285224.
Tornberg, A.K., Shelley, M.J., 2004. Simulating the dynamics and interactions of flexible fibres in Stokes flows. J. Comput. Phys. 196, 8–40.
Usta, O.B., Ladd, A.J.C., Butler, J.E., 2007. Transverse migration of a confined polymer driven by an external force. Phys. Rev. Lett. 98, 098301.
Yamamoto, S., Matsuoka, T., 1993. A method for dynamic simulation of rigid and flexible fibres in a flow field. J. Chem. Phys. 98, 644–650.
Zurita-Gotor, M., Blawzdziewicz, J., Wajnryb, E., 2007. Motion of a rod-like particle between parallel walls with application to suspension rheology. J. Rheol. 51, 71–97.